

Inclusive charmonium production at PANDA experiment

A.V. Luchinsky^{1,*} and S.V. Poslavsky^{1,†}

¹*Institute for High Energy Physics, Protvino, Russia*

The production of the charmonium states in $p\bar{p}$ experiments is considered at the energy rates near threshold in NLO. Such a consideration allows one to obtain non zero distributions over the transverse momentum of the final charmonium and gives a natural explanation to the existence of χ_{c1} -meson in final state, that is observed experimentally and cannot be produced in leading order processes. The crucial role of scale parameter choice in $\alpha_s(Q^2)$ and partonic distributions $f(x, Q^2)$ shown, and the correct choice offered.

PACS numbers: 13.75.-n, scattering (energy ≥ 10 GeV) 13.60.Le, 14.40.Pq

I. INTRODUCTION

Precision experimental studies of the charmonium production in proton-antiproton collisions at low energies proposed in new experiment, labeled PANDA [1]. Such studies allows to obtain a deeper understanding of charmonium physics. PANDA experiment deals with proton target and antiproton beam energies up to 15 GeV. This energies lies near charmonium production threshold. In present article we give a theoretical predictions of the inclusive charmonium production in $p\bar{p}$ collisions by accounting next to leading order diagrams in partonic cross sections. Such an approach was considered by a number of authors [2, 8–10] and applied mainly for proton-proton collisions.

The important part of the Program is the detailed analysis of all possible mechanisms of charmonia production. Such an analysis is especially important since at low energies there is significant difference between charmonium production in $p\bar{p}$ and pp . For the pp at low energies the contributions of gluon-gluon, quark-gluon and quark-antiquark subprocesses are comparable, while for $p\bar{p}$ the quark-antiquark annihilation subprocess dominates. For example, if the energy of the proton beam is equal to 40 GeV, the ratio of ψ production

* Alexey.Luchinsky@ihep.ru

† stvlpos@mail.ru

cross sections in $p\bar{p}$ and pp collisions equals $\sigma(p\bar{p})/\sigma(pp) \sim 6$.

Another problem is that the direct production of ψ -meson is suppressed in comparison with the production of the intermediate P -wave states $\chi_{c0,1,2}$ with the subsequent decay $\chi_c \rightarrow J/\psi\gamma$. This fact is well confirmed in the experiments [3]. The experimentally observed cross sections of χ_{c2} and χ_{c1} are comparable (χ_{c0} -meson can hardly be observed due to its small radiative width), while the well known Landau-Yang theorem forbids the formation of the axial meson from two massless gluons. One more difficulty is that the partonic distributions are integrated over the transverse momentum. As a result, such method does not allow one to obtain the distributions of χ_{c0} - and χ_{c2} -mesons over p_T .

Initially this problems were solved by the introduction of color-octet (CO) components of the quarkonia, that arise naturally in the non-relativistic quantum chromodynamics (NRQCD), where the expansion over the relative velocity of quarks in meson is performed. In this model it is assumed, that final meson is formed from heavy quark pair in color-octet state, that subsequently transforms into a physically observed colorless meson. In the framework of NRQCD the probabilities of these transitions are described by the matrix elements of four-fermion operators, that are determined from the experimental distributions over the transverse momentum of final charmonium. We would like to stress, however, that this explanation will not work for charmonium production at lower energies. The reason is that the distributions caused by octet components decreases slowly with the rise of the transverse momentum, but the probability to find such a component in the meson is small, compared with the singlet case. As a result, in the large transverse momentum region the contribution of octet components can be significant, but for small energies and transverse momenta it is suppressed.

Recently another way to solve this problem was proposed, where the so called non-integrated over the transverse momentum distribution functions $G(x, k_T)$ are used (k_T -factorization) [13–15]. In this case both mentioned above problems are solved simultaneously. The transverse momentum of the produced in gluon fusion $\chi_{c0,2}$ mesons is explained by the transverse momenta of the initial partons. Axial charmonium meson can also be produced in gluon fusion, since in the framework of k_T factorizations gluons have non-zero virtuality of the order k_T^2 . There is a number of works, that explain the experimental distributions on TEVATRON with the help of these functions (see, for example [14, 16, 17]). According to these works, there is no need to introduce CO components to reproduce the experi-

mental data on P -wave charmonium p_T distributions. Thus, in k_T -factorization approach color-singlet components give the main contribution.

Unfortunately, the method, used in the modeling of the unintegrated distribution functions $G(x, k_T)$, is based on the summation of large $\log(1/x)$, so it is not applicable for low energies, where the gluon momentum fractions are in the range $0.1 < x_g < 0.5$. For this reason we are forced to use the following approximation in our calculations. We start from the collinear gluon distributions with well known collinear distribution functions. Further we consider the charmonia production at next to leading (NLO) order in the strong coupling constant α_s . Such a trick enables us to obtain the distributions over p_T for all charmonium states. For χ_{c0} and χ_{c2} production we observe a collinear singularity at $p_T = 0$. To avoid this singularity we introduce a regularization procedure. For directly produced ψ and χ_{c1} such a singularity is absent and we use the whole integration region for p_T .

Next section is devoted to the consideration of different modes of charmonia production and collinear singularities regularization. In the third section we determine the cross sections of the hadronic processes and pay attention to the correct scale parameters choice in $\alpha_s(Q^2)$ and parton distributions $f(x, Q^2)$. There we are present numerical results.

II. PARTONIC SUBPROCESSES

Feynman diagrams corresponding to the charmonium production are presented in Fig.1. At the leading (Fig.1a) order only processes $gg \rightarrow \chi_{c0,2}$ are available. Process $gg \rightarrow \psi$ is forbidden by charge parity. Process $gg \rightarrow \chi_{c1}$ is forbidden due to Landau-Yang theorem, that forbids the formation of the axial meson from two massless gluons. Other LO cross sections we give in Appendix A.

Next to leading order diagrams are presented in Fig.1b,c. First two diagrams in Fig.1c includes 3-gluon vertex. To avoid delicate problems, bounded with ghosts contributions, we recalculated differential cross sections for process $gg \rightarrow Qg$ ($Q = \psi, \chi_{c0,1,2}$) (and also for $qg \rightarrow \chi_{0,1,2}q$) in axial gauge:

$$\mathcal{L}_{gf} = -\frac{1}{2\xi}(n_\mu A^{a\mu})^2, \text{ with } n_\mu n^\mu = -1 \quad (1)$$

This gauge does not require additional ghosts Lagrangian, but gluon propagator and polarization sum becomes more complicated. Using $\xi = 0$ (Landau choice), it can be found

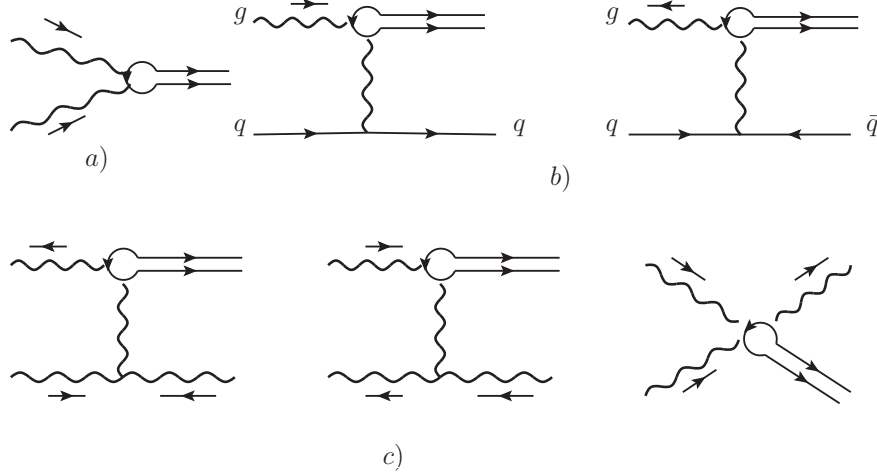


Figure 1. Feynman diagrams for the charmonium production. a) direct $\chi_{c0,2}$ production. b) through $qg \rightarrow \mathcal{Q}q$ and $\bar{q}q \rightarrow \mathcal{Q}g$ subprocesses, where $\mathcal{Q} = \chi_{cJ}$. c) through $gg \rightarrow \mathcal{Q}g$ subprocess, where $\mathcal{Q} = \chi_{cJ}$ for the first two diagrams and $\mathcal{Q} = \psi, \chi_{cJ}$ for the last diagram.

that

$$\begin{aligned} \sum \epsilon_\mu(k) \epsilon_\nu(k) &= -\eta_{\mu\nu} + \frac{k_\mu k_\nu}{(k, n)^2} - \frac{k_\mu n_\nu + k_\nu n_\mu}{(k, n)}, \\ D_{\mu\nu}^{ab}(k) &= \delta^{ab} \frac{1}{k^2} \sum \epsilon_\mu(k) \epsilon_\nu(k) \end{aligned} \quad (2)$$

Auxiliary vector n_μ will disappear in physical observables. We found, that our results are in excellent agreement with [9], [10] for gg channel and [2] for qg channel. Exact formulas for the differential cross sections are rather tedious and can be found in the cited papers.

Massless \hat{t} -channel gluon in propagators in Fig.1 leads to the collinear singularities in small \hat{t} and $\hat{u} = M^2 - \hat{s} - \hat{t}$ regions, so $gg \rightarrow \chi_{0,2}g$ and $qg \rightarrow \chi_{0,2}q$ are divergent:

$$\frac{d\hat{\sigma}}{d\hat{t}} \sim \frac{1}{\hat{t}\hat{u}}. \quad (3)$$

In terms of meson transverse momentum $p_T = \sqrt{\hat{t}\hat{u}/\hat{s}}$, these singularities correspond to $p_T \rightarrow 0$ singularity. To calculate the total cross section:

$$\hat{\sigma}(\hat{s}) = \int_{M^2 - \hat{s}}^{\hat{t}} d\hat{t} \frac{d\hat{\sigma}(\hat{s}, \hat{t})}{d\hat{t}} = \int_0^{(\hat{s} - M^2)/2\sqrt{\hat{s}}} dp_T \frac{d\hat{\sigma}(\hat{s}, p_T)}{dp_T}, \quad (4)$$

some regularization should be performed. Popular decision is to cut off the small p_T region, i.e. restrict integration region in last formula by setting $p_T > \Delta$, where cutoff parameter Δ

can be taken from experimental setup or from some physical reasons. For example in [2], Δ was taken equal to $1/R_{c\bar{c}}$, where $R_{c\bar{c}}$ is the geometrical size of charmonium. Such approach have a big lack, because the total cross section is high sensitive to Δ variation. To avoid these difficulties, we will use another regularization procedure.

Taking indefinite integral of differential cross section, the following well known relation can be found:

$$\int d\hat{t} \frac{d\hat{\sigma}(gg \rightarrow Qg)}{d\hat{t}} = \frac{\alpha_s}{2\pi} \hat{\sigma}_0(gg \rightarrow Q) P_{g \rightarrow gg} \left(\frac{M^2}{\hat{s}} \right) \ln \frac{\hat{u}}{\hat{t}} + \text{finite} \quad (5)$$

Similarly, for $qg \rightarrow Qq$ reaction we have

$$\int d\hat{t} \frac{d\hat{\sigma}(qg \rightarrow Qq)}{d\hat{t}} = \frac{\alpha_s}{2\pi} \hat{\sigma}_0(qg \rightarrow Q) P_{q \rightarrow qg} \left(\frac{M^2}{\hat{s}} \right) \ln \frac{\hat{u}}{\hat{t}} + \text{finite}. \quad (6)$$

In these expressions the second parts are finite at $\hat{t} \rightarrow 0$ and $\hat{t} \rightarrow M^2 - \hat{s}$, while $\hat{\sigma}_0(gg \rightarrow Q)$ are given in (A2), (A2). $P_{g \rightarrow gg}(x)$ and $P_{q \rightarrow qg}(x)$ are well known QCD splitting functions:

$$P_{g \rightarrow gg}(x) = 6 \left(\frac{x}{1-x} + \frac{1-x}{x} + x(1-x) \right)$$

$$P_{q \rightarrow qg}(x) = \frac{4}{3} \frac{1 + (1-x)^2}{x}$$

The full hadronic cross section can be obtained by integrating partonic cross sections with partonic distribution functions:

$$\sigma(s) = \int dx_1 dx_2 f(x_1) f(x_2) \hat{\sigma}(\hat{s}) \quad (7)$$

Singular parts of (5) and (6) are included in partonic distributions functions $f(x)$ and generate well known scaling violations, described by Altarelli-Parisi equations. So, inclusion of singular parts in partonic cross sections leads to double-counting: one time in $\hat{\sigma}$ and one in $f(x)$. Thus, we will use regularization:

$$\hat{\sigma}^{Reg}(gg \rightarrow Qg) = \left(\int \frac{d\hat{\sigma}(gg \rightarrow Qg)}{d\hat{t}} d\hat{t} - \frac{\alpha_s}{2\pi} \hat{\sigma}_0(gg \rightarrow Q) P_{g \rightarrow gg} \left(\frac{M^2}{\hat{s}} \right) \ln \frac{\hat{u}}{\hat{t}} \right) \Bigg|_{\hat{t}=M^2-\hat{s}}^{\hat{t}=0} \quad (8)$$

and similarly:

$$\hat{\sigma}^{Reg}(qg \rightarrow Qq) = \left(\int \frac{d\hat{\sigma}(qg \rightarrow Qq)}{d\hat{t}} d\hat{t} - \frac{\alpha_s}{2\pi} \hat{\sigma}_0(qg \rightarrow Q) P_{q \rightarrow qg} \left(\frac{M^2}{\hat{s}} \right) \ln \frac{\hat{u}}{\hat{t}} \right) \Bigg|_{\hat{t}=M^2-\hat{s}}^{\hat{t}=0} \quad (9)$$

In contrast to $\chi_{c0,2}$, differential cross sections for ψ and χ_{c1} have no collinear singularities and finite at $\hat{t} \rightarrow 0$ and $\hat{u} \rightarrow 0$. In case of χ_1 , this is explained by the Landau-Yang theorem,

that forbids the production from two massless gluons. As a result, the squared matrix element of this reaction is proportional to the virtuality of the intermediate t-channel gluon, so this factor compensates the divergency, caused by the propagator. For ψ , we have similar reasoning based on charge parity, since the first two diagrams of Fig.1c are absent in this case.

Exact formulas for regularized partonic cross sections are given in Appendix A

III. HADRONIC CROSS SECTIONS

Let us now consider full hadronic process

$$A(P_1)B(P_2) \rightarrow \mathcal{Q}(P) + X, \quad (10)$$

where A and B are the initial hadrons, $\mathcal{Q} = \psi, \chi_{cJ}$, and in the parentheses corresponding particle momenta introduced. The cross section of this reaction is expressed through the cross sections of considered above partonic reactions :

$$\sigma(s) = \sum_{a,b} \int dx_1 dx_2 f_{a/A}(x_1) f_{b/B}(x_2) \hat{\sigma}_{ab}(\hat{s}), \quad (11)$$

where summation is performed over partons a and b , $x_{1,2}$ are the momentum fractions held by these partons, and $f_{a/A}(x_1)$, $f_{b/B}(x_2)$ are the distribution functions of the partons in the initial hadrons. In the common variables

$$x = x_1 - x_2 \quad (12)$$

$$\hat{s} = (x_1 P_1 + x_2 P_2)^2 = x_1 x_2 s, \quad (13)$$

the full hadronic cross-section becomes

$$\sigma(s) = \sum_{a,b} \int_{M^2}^s d\hat{s} \hat{\sigma}_{ab}(\hat{s}) \int_{-x(\hat{s})}^{x(\hat{s})} \frac{dx}{\tilde{x}} f_{a/A}(x_1) f_{b/B}(x_2) \Big|_{x_{1,2}=x_{1,2}(x,\hat{s})}, \quad \tilde{x} = x_1 + x_2, \quad (14)$$

where

$$x(\hat{s}) = 1 - \frac{\hat{s}}{s} \quad (15)$$

In our numerical estimates we used the distribution functions and α_s numeric values presented in the work [11]. Other numerical parameters are equal to:

$$M_\psi = 3.097 \text{ GeV}, \quad M_{\chi_{c0}} = 3.415 \text{ GeV}, \quad (16)$$

$$M_{\chi_{c1}} = 3.511 \text{ GeV}, \quad M_{\chi_{c2}} = 3.556 \text{ GeV} \quad (17)$$

$$R_S^2(0) = 0.81 \text{ GeV}^3, \quad R_P^{\prime 2}(0) = 0.075 \text{ GeV}^5 \quad (18)$$

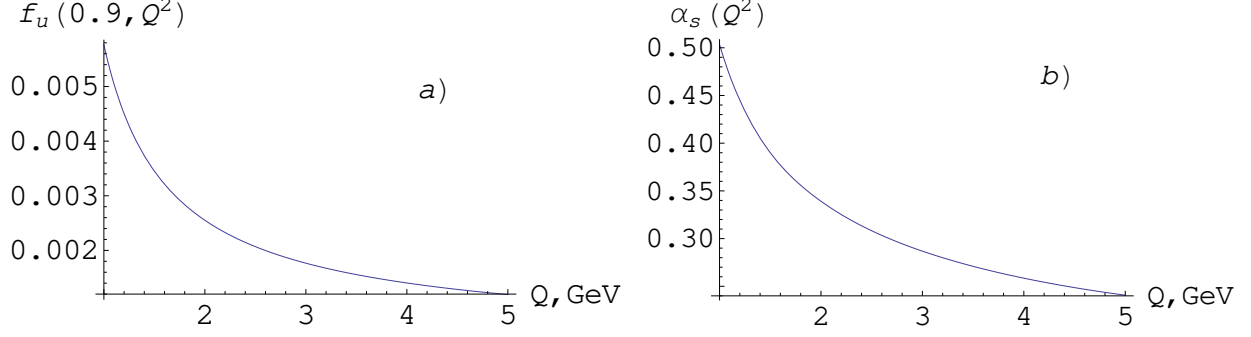


Figure 2. a) Q -dependence of u -quark distribution at $x = 0.9$ b) Q -dependence of α_s

A. Scale dependence

There are two physical quantities, that depend on some scale choice: partons distributions $f_{a/A}(x, Q^2)$ and strong coupling constant $\alpha_s(Q^2)$. The parton distribution function $f_{a/A}(x, Q^2)$, gives the probability of finding a parton a of longitudinal fraction x in physical (anti)proton, taking into account collinear gluon (or massless quark) with transverse momenta $p_T < Q$. It is clear, that exact value of Q depends on parameters of partonic subprocess, i.e. $Q^2 = Q^2(\hat{s})$. It is convenient to set Q^2 to a fixed value Q_*^2 - characteristic momentum transfer of partonic subprocess. Such choice can be argued by mean value theorem, which states:

$$\int_a^b f(x)g(x)dx = f(x_*) \int_a^b g(x)dx$$

On the other hand, from the structure of Altarelli-Parisi equations, it is clear, that at least for high energies ($Q \gg 1$ GeV) error in choosing of Q_* leads to negligibly small variation of final results; for example, the parton distributions change by $\sim 1\%$ as Q_* is changed by a factor of 10. Another situation we have at low energies ($Q \ll 1$ GeV), when perturbation theory works bad, and error in choosing of Q_* leads to a dramatic variation of partonic functions. At the energy rates ~ 1 GeV, error in Q_* in two times can leads to $f(x, Q_*^2)$ error about 20%. For example, u-quark distribution dependence on Q_* is shown on Fig.2 a).

Second physical quantity, depending on some scale choice is $\alpha_s(Q^2)$. Here, the meaning of Q is different from the meaning in distribution functions. The strong coupling α_s scale dependence occurs when the full propagators and vertexes are inserted in tree level diagrams. Similar reasoning, based on mean value theorem allows to set $\alpha_s(Q^2)$ to a fixed value with

some scale Q_* . The perfect justification of this procedure is given in [12]. Only in simplest situations the exact value of Q_* can be found: for example for $2 \rightarrow 2$ reaction through s -channel particle, it can be found, using Callan-Symanzik renorm-group equation, that $Q_*^2 = s$. In other cases the exact value of scale can be found only by sequential analysis of perturbation series expansion. It is clear, that Q_* depends on the process. At high energies $Q \gg 1 \text{ GeV}$ $\alpha_s(Q^2)$ becomes almost constant. At the energies rates near 1 GeV, α_s dependence of Q is shown on Fig.2 b).

So, in general, we have three possible ways of setting scale parameters in full cross section:

$$\begin{aligned} \text{fixed scheme} \quad \sigma(s, Q_*^2) &= \sum_{a,b} \int_{M^2}^s d\hat{s} \hat{\sigma}_{ab}(\hat{s}, \alpha_s(Q_*^2)) \int_{-x(\hat{s})}^{x(\hat{s})} \frac{dx}{\hat{x}} f_{a/A}(x_1, Q_*^2) f_{b/B}(x_2, Q_*^2) \\ \text{float scheme} \quad \sigma(s, Q_*^2) &= \sum_{a,b} \int_{M^2}^s d\hat{s} \hat{\sigma}_{ab}(\hat{s}, \alpha_s(\hat{s})) \int_{-x(\hat{s})}^{x(\hat{s})} \frac{dx}{\hat{x}} f_{a/A}(x_1, Q_*^2) f_{b/B}(x_2, Q_*^2) \\ \text{float2 scheme} \quad \sigma(s, Q_*^2) &= \sum_{a,b} \int_{M^2}^s d\hat{s} \hat{\sigma}_{ab}(\hat{s}, \alpha_s(\hat{s})) \int_{-x(\hat{s})}^{x(\hat{s})} \frac{dx}{\hat{x}} f_{a/A}(x_1, \hat{s}) f_{b/B}(x_2, \hat{s}) \end{aligned}$$

The fixed scheme is the most common way, used in calculations. The float scheme, takes in account the fact, that α_s in partonic subprocess, depends on \hat{s} . Of course, in general, this dependence is complicated and has the form $\alpha_s(f(\hat{s}))$, but from general considerations it is clear, that for small interval, near process threshold, $f(\hat{s}) \sim \hat{s}$. The float2 scheme, takes in account both $\alpha_s(Q^2)$ and $f(x, Q^2)$ scaling. It is also clear that maximum transverse momentum Q in $f(x, Q^2)$ depends on the \hat{s} and for small energy intervals we set $Q^2 \sim \hat{s}$. Actually, the cross section in float2 scheme does not depends on Q_* .

Fig.3 illustrates the dependence of the cross section on scheme choice for χ_{c0} production in $u\bar{u}$ channel at $p\bar{p}$ collisions. It is seen, that all three curves are crossed in one point at $Q^2 = M_{\chi_{c0}}^2 = 11.66 \text{ GeV}^2$. For other mesons and other channels the picture is equivalent - three curves are crossed at the corresponding squared meson mass. The only exception — quark-gluon channel, where cross point greater at 10%, then corresponding squared meson mass (Fig.4). We make similar calculations for other energy regions and found, that this results remain valid. As was expected, at high energies ($s \gg 1 \text{ GeV}^2$) the difference between schemes is negligible. So, this results improves that all schemes are equivalent with the correct Q_* choice:

$$Q_* = M, \tag{19}$$

where M - corresponding meson mass.

In all further calculations we shall use the fixed scheme with $Q_* = M$.

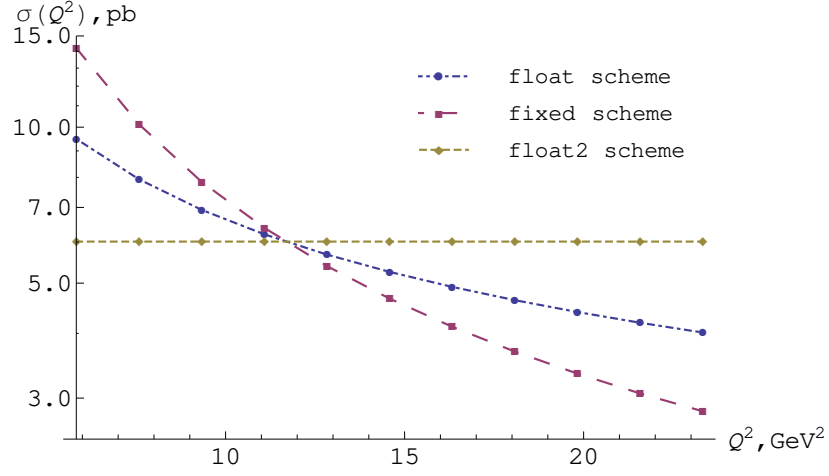


Figure 3. Scale dependence in different schemes of the $u\bar{u}$ channel cross section in $p\bar{p} \rightarrow \chi_{c0}X$ collision at the energy $\sqrt{s} = 4.34\text{GeV}$.

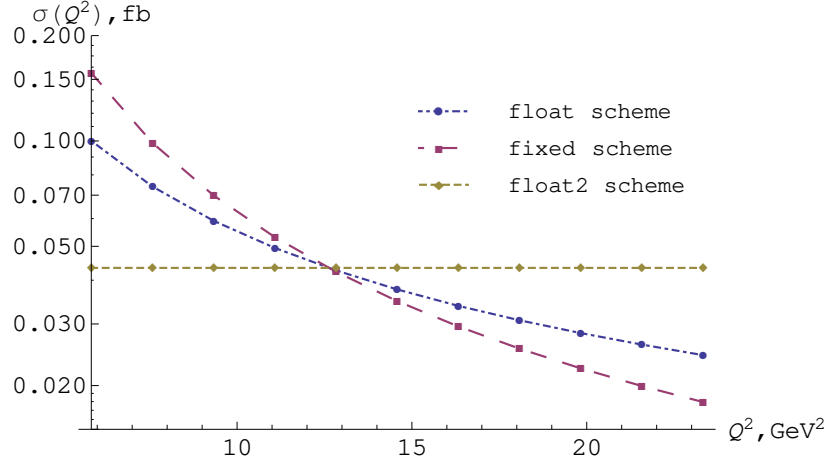


Figure 4. Scale dependence in different schemes of the ug channel cross section in $p\bar{p} \rightarrow \chi_{c0}X$ collision at the energy $\sqrt{s} = 4.34\text{GeV}$.

B. Total cross sections

Fig.5 illustrates the dependence of ψ production through different processes on total energy. The bold line shows the summed over all processes cross section:

$$\sigma = \sigma_{gg}(\psi) + \text{Br}(\chi_{c0} \rightarrow \psi\gamma)\sigma(\chi_{c0}) + \text{Br}(\chi_{c1} \rightarrow \psi\gamma)\sigma(\chi_{c1}) + \text{Br}(\chi_{c2} \rightarrow \psi\gamma)\sigma(\chi_{c2}), \quad (20)$$

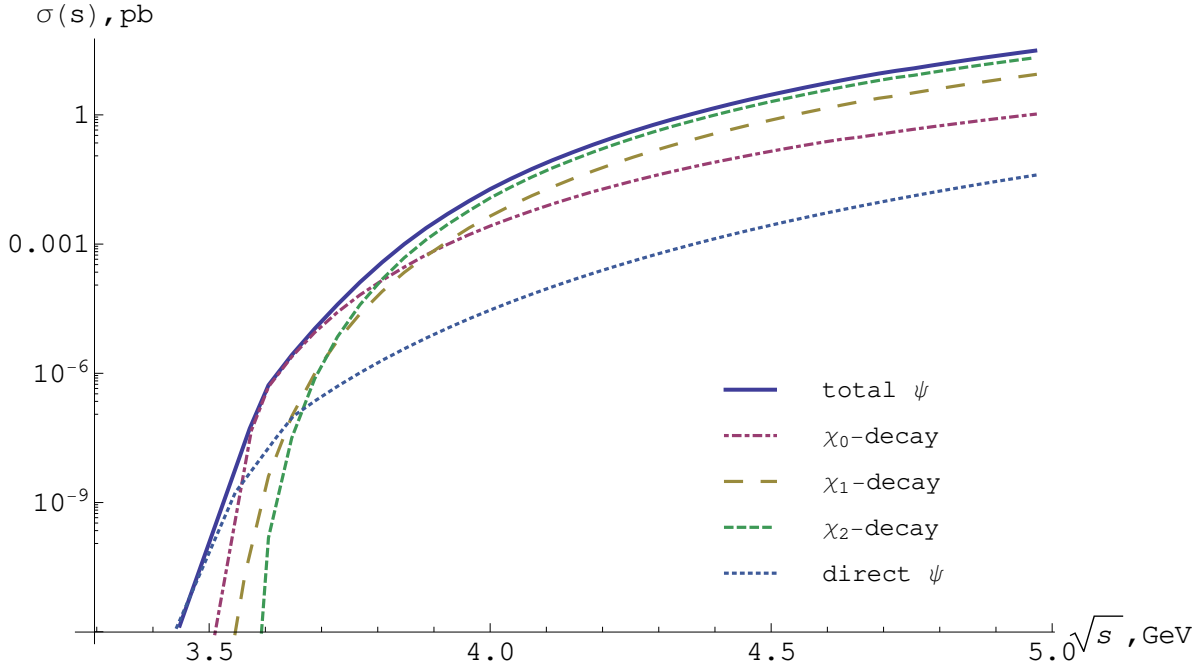


Figure 5. Different contributions to the total ψ production in proton-antiproton reaction for different c.m. energies. 1 — total ψ production, 2 — ψ production through the radiative χ_{c2} decay, 3 — through the radiative χ_{c1} decay, 4 — through the radiative χ_{c0} decay, 5 — direct ψ .

where the branching values are equal to:

$$\text{Br}(\chi_{c0} \rightarrow \psi\gamma) = 0.016, \quad \text{Br}(\chi_{c1} \rightarrow \psi\gamma) = 0.344, \quad \text{Br}(\chi_{c2} \rightarrow \psi\gamma) = 0.195 \quad (21)$$

From this picture it is seen, that direct ψ production and production from radiative χ_{c0} decay is highly suppressed. The contribution of χ_{c0} radiative decay is negligible, due to very small branching value. As was noted above, the direct ψ production only available in process $gg \rightarrow \psi g$, but the gluon-gluon channel in $p\bar{p}$ reactions is highly suppressed by the quark-antiquark channel, so the cross section of the direct ψ production is significantly smaller, then the production of χ_{cJ} , where the quark-antiquark channel is available.

In the Fig.6 and Fig.7 we show the contributions of the different subprocesses to the total χ_{c1} and χ_{c2} production cross sections. For both mesons the most significant contribution gives the $u\bar{u}$ subprocess. For the gluon-gluon subprocess our numerical results are equals to zero within the error of numerical calculations. The negligibly small effect of the other channels can be easily explained by the structure of the parton distributions. The small

energy of the hadronic reaction corresponds to the longitudinal fraction x in partonic distributions $f_{a/A}(x)$ close to zero. For this region the u -quark distribution function absolutely dominates.

C. Production mode at the $s = 32 \text{ GeV}^2$

It should be stressed, that presented above expressions for charmonia production cross sections can be considered only as estimates on upper bounds. The reasons is that in some events initial (anti)protons are present also in the final state. Due to baryonic number conservation in proton-proton scattering this configuration is realized almost always. In proton-antiproton interaction, however, that presence of baryons in the final state is not necessary. Numerically this effect can be described in terms of inelasticity coefficient, which can be interpreted as the probability of proton-antiproton annihilation into other states. According to presented in [18] analysis, this coefficient is equal to $K \sim 0.5$ and decreases slightly with the increase of energy.

If initial baryons are present also in the final state, the effective interaction energy decreases from \sqrt{s} to $\sqrt{s_{\text{eff}}} \sim \sqrt{s} - 2M_p$. In the case of high-energy colliders this modification does not change significantly the cross sections of the considered processes. For PANDA environment, however, situation is completely different. From fig.5 it is clear, that the decrease from $\sqrt{s} \sim 5.5 \text{ GeV}$ to $\sqrt{s_{\text{eff}}} \sim 3.5 \text{ GeV}$ leads to dramatic decrease of charmonia production cross sections. So, one can expect, that the reactions $p\bar{p} \rightarrow p\bar{p} + J/\psi + X$ give negligible contributions to the cross sections of charmonia production at PANDA, and expression (14) should be multiplied by the inelasticity factor $K \sim 0.5$.

At the production mode in PANDA experiment the antiproton beam energy equals to 15 GeV , that corresponds to the s value equals to 32 GeV^2 . The cross section of ψ meson production is given in (20). Our calculations give

$$\sigma(p\bar{p} \rightarrow \psi X) = 0.21 \text{ nb}, \quad (22)$$

where

$$\begin{aligned} \sigma(p\bar{p} \rightarrow \chi_{c1} X) &= 0.2 \text{ nb} \\ \sigma(p\bar{p} \rightarrow \chi_{c2} X) &= 0.75 \text{ nb} \\ \sigma(p\bar{p} \rightarrow \chi_{c0} X) &= 0.35 \text{ nb}. \end{aligned}$$

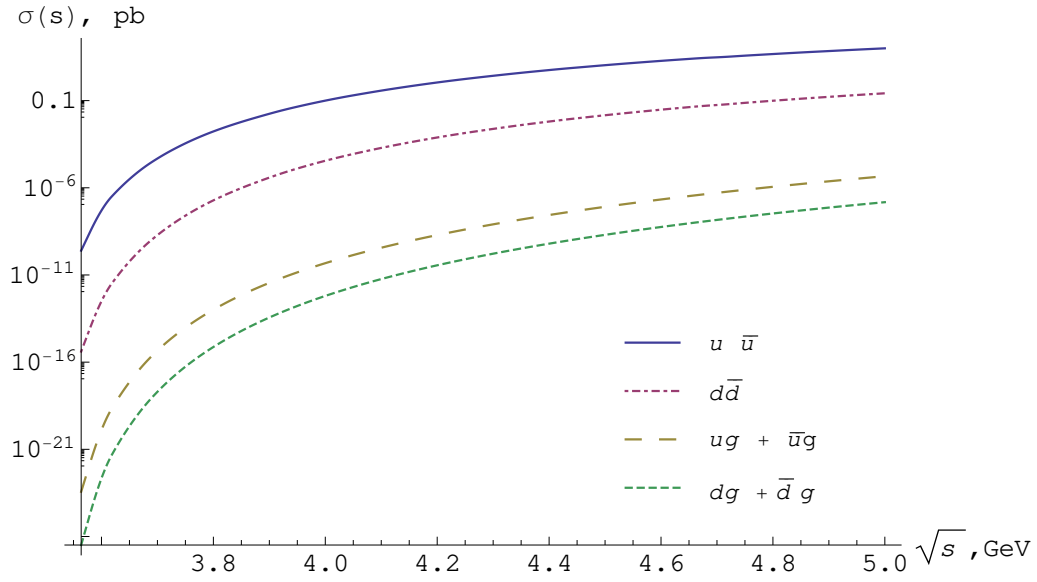


Figure 6. Contribution of the different subprocesses to the total χ_{c1} production. 1 — $u\bar{u}$ subprocess, 2 — $d\bar{d}$ subprocess, 3 — the sum over ug and $\bar{u}g$ subprocesses, 4 — the sum over dg and $\bar{d}g$ subprocesses.

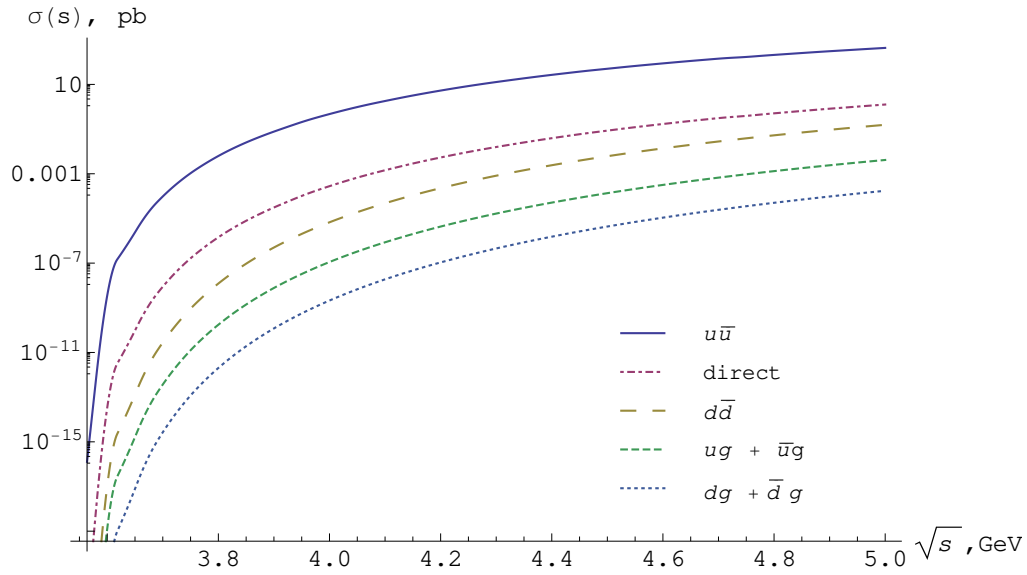


Figure 7. Contribution of the different subprocesses to the total χ_{c2} production. 1 — $u\bar{u}$ subprocess, 2 — direct χ_{c2} , 3 — $d\bar{d}$ subprocess, 4 — the sum over ug and $\bar{u}g$ subprocesses, 5 — the sum over dg and $\bar{d}g$ subprocesses.

The ratio of χ_{c1} and χ_{c2} production cross sections is equal to

$$\frac{\sigma(\chi_{c1})}{\sigma(\chi_{c2})} = 0.26 \quad (23)$$

The p_T distribution of mesons, can be obtained by rewriting differential cross sections in terms of $p_T = \sqrt{\hat{t}\hat{u}/\hat{s}}$ and integrating with the partonic distributions:

$$\frac{d\sigma}{dp_T} = \int_{(p_T + \sqrt{p_T^2 + M^2})^2}^s \frac{d\hat{s}}{s} \frac{d\hat{\sigma}(ab \rightarrow \mathcal{Q}c)}{dp_T} \int_{-(1-\frac{\hat{s}}{s})}^{1-\frac{\hat{s}}{s}} \frac{dx}{\tilde{x}} f_{a/A}(x_1) f_{b/B}(x_2) \quad (24)$$

where

$$\begin{aligned} \frac{d\hat{\sigma}}{dp_T} &= \frac{2\hat{s}p_T}{\sqrt{(\hat{s} - M^2)^2 - 4\hat{s}p_T^2}} \left(\left. \frac{d\hat{\sigma}}{d\hat{t}} \right|_{\hat{t}=\hat{t}_1} + \left. \frac{d\hat{\sigma}}{d\hat{t}} \right|_{\hat{t}=\hat{t}_2} \right), \\ \hat{t}_{1,2} &= \frac{1}{2}(M^2 - \hat{s} \pm \sqrt{(\hat{s} - M^2)^2 - 4\hat{s}p_T^2}) \end{aligned}$$

As was shown before, the major processes, giving contribution to the total ψ production, are the radiative decays of the $\chi_{c1,2}$ mesons, which in turn are formed through the $u\bar{u}$ subprocess. Thus, for the calculation of the p_T dependence we will neglect all other channels of the ψ production. In this approximation we do not encounter with collinear singularities, that appear in other subprocesses of χ_{c2} formation. Another problem arises when we consider the total ψ distribution. The radiative decays $\chi_{cJ} \rightarrow \psi\gamma$ can give significant contribution to the p_T -distribution of the final ψ , when the transverse momentum ~ 1 GeV. However, we will neglect such contribution. On the Fig.8 we show the transverse momentum distributions of the ψ production:

$$\begin{aligned} \frac{d\sigma(\chi_{c1,2})}{dp_T} &= \int \frac{d\hat{s}}{s} \frac{d\hat{\sigma}(u\bar{u} \rightarrow \chi_{c1,2}g)}{dp_T} \int \frac{dx}{\tilde{x}} f_{u/p}(x_1) f_{\bar{u}/\bar{p}}(x_2), \\ \frac{d\sigma(\psi)}{dp_T} &= \text{Br}(\chi_{c1} \rightarrow \psi\gamma) \frac{d\sigma(\chi_{c1})}{dp_T} + \text{Br}(\chi_{c2} \rightarrow \psi\gamma) \frac{d\sigma(\chi_{c2})}{dp_T} \end{aligned}$$

IV. CONCLUSIONS

The paper is devoted to J/ψ -meson production in proton-antiproton interaction at low energies. This process can be used to clarify modes of charmonia production in hadronic experiments and allows one to measure with higher accuracy proton spectral functions at $x \sim 0.5$.

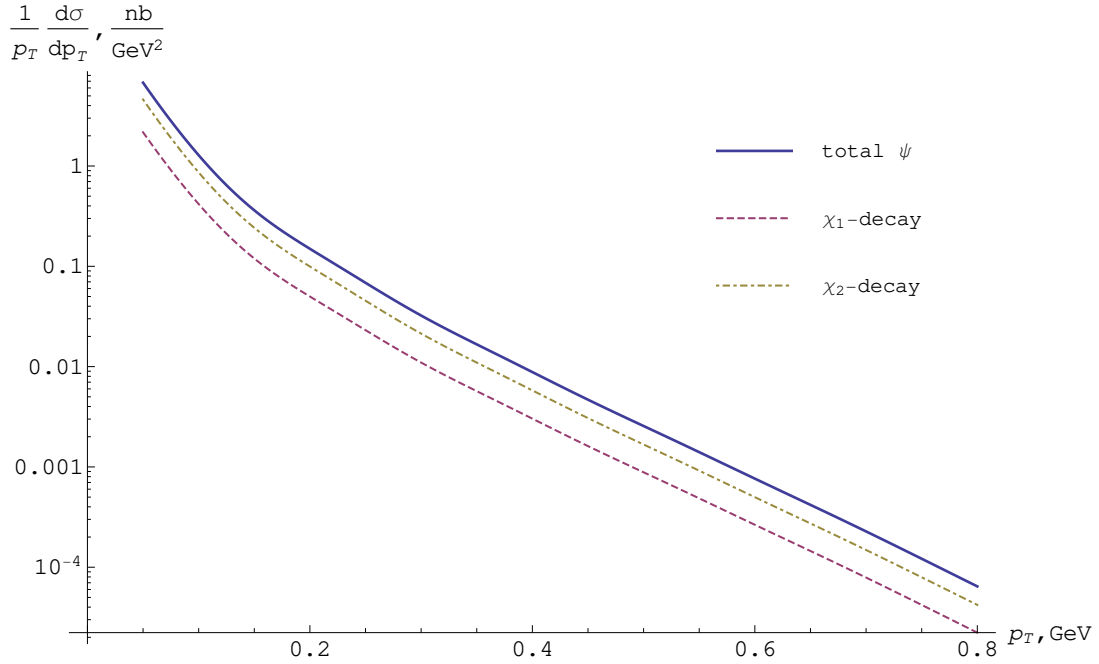


Figure 8. Transverse momentum distributions of ψ production with inelasticity coefficient taken into account. 1 — total ψ , 2 — ψ production through χ_{c2} decay, 3 — ψ production through χ_{c1} decay

The physics of charmonia production in hadronic reactions is completely different for different energies. For high-energy experiments (e.g. Tevatron or LHC) heavy quarkonia are produced mainly in the gluon-gluon interaction, since small values of feynman variable x are allowed kinematically. The contributions of quark-gluon or quark-antiquark modes are negligible. In the threshold region, where only values $x \sim 0.5$ are allowed, on the contrary, main contributions come from quark-gluon (in proton-proton interaction) or quark-antiquark (in the proton-antiproton interactions). In the nearest future at the FAIR proton-antiproton particle accelerator with $3 < \sqrt{s} < 5.7$ GeV the PANDA detector will perform first measurements, so a reliable prediction for charmonium mesons production for this experiment is required.

In our paper we give predictions for total cross sections of J/ψ -meson production in different modes at NLO. The emission of additional gluon leads to non-zero transverse momentum of final charmonium, that is obviously absent in LO partonic reactions $gg \rightarrow \chi_{c0,2}$. It is shown, that main contributions to this process are given by $\chi_{c1,2}$ -mesons production due to quark-antiquark annihilation with the subsequent radiative decay $\chi_{c1,2} \rightarrow J/\psi\gamma$.

Special attention is given to regularization of infrared and collinear singularities in the case of χ_{c2} meson production, when the t -channel gluon in $gg \rightarrow \chi_{c2}g$ partonic reactions leads to divergency in p_T distribution and infinitive values of the cross section.

ACKNOWLEDGMENTS

The authors would like to thank A.K. Likhoded for useful discussions. Also, authors would like to thank experimentators group: V.V. Mochalov, A.N. Vasiliev and D.A. Morozov for introduction in PANDA facilities.

This research is partially supported by Russian Foundation for Basic Research (grant 10-02-00061a). The work of A. V. Luchinsky was also supported by non-commercial foundation Dynasty and the grant of the president of Russian Federation for young scientists with PhD degree (grants MK-406.2010.2, MK-3513.2012.2).

Appendix A: Regularized partonic cross sections

In this section we give the total cross sections of partonic subprocesses. For subprocesses, in which the collinear singularities appears, we use the regularization procedure, described in the main text.

1. Leading order

In the leading order only $gg \rightarrow \chi_{c0,2}$ reactions are possible. The cross sections of these reactions are

$$\hat{\sigma}(gg \rightarrow Q) = \hat{\sigma}_0(gg \rightarrow Q)\delta(1 - M^2/\hat{s}), \quad (\text{A1})$$

where

$$\begin{aligned} \hat{\sigma}_0(gg \rightarrow \chi_0) &= 12 \frac{\pi^2 \alpha^2 R'_\chi{}^2(0)}{M^5 \hat{s}}, \\ \hat{\sigma}_0(gg \rightarrow \chi_2) &= 16 \frac{\pi^2 \alpha^2 R'_\chi{}^2(0)}{M^5 \hat{s}}, \end{aligned}$$

where $R'_\chi(0)$ is the derivative of the radial part of χ -meson wave function at the origin,

2. $gg \rightarrow Qg$

As was noted above, the cross sections for processes $gg \rightarrow \psi g$ and $gg \rightarrow \chi_{c1} g$ have no collinear singularities, so they does not require regularization/ We have

$$\hat{\sigma}(gg \rightarrow \psi g) = -\frac{10\pi\alpha^3 R_\psi(0)^2}{9\hat{s}^2 (M^2 - \hat{s})^2 (M^2 + \hat{s})^3} \left(M^{10} + 4M^8\hat{s} - 2M^4\hat{s}^3 - M^2\hat{s}^4 - \right.$$

where $R_\psi(0)$ is the radial part of ψ wave function at the origin, and

$$\begin{aligned} \hat{\sigma}(gg \rightarrow \chi_{1g}) = & \frac{4\pi\alpha^3 R_\chi'^2(0)}{M^7\hat{s}^2 (M^2 - \hat{s})^4 (M^2 + \hat{s})^5} \left(12M^4\hat{s} \left(M^{16} + 9M^{14}\hat{s} + \right. \right. \\ & 26M^{12}\hat{s}^2 + 28M^{10}\hat{s}^3 + 17M^8\hat{s}^4 + 7M^6\hat{s}^5 - 40M^4\hat{s}^6 - 4M^2\hat{s}^7 - 4\hat{s}^8 \Big) \log \frac{M^2}{\hat{s}} - \\ & (M^2 - \hat{s})(M^2 + \hat{s}) \left(M^{18} + 39M^{16}\hat{s} + 145M^{14}\hat{s}^2 + 251M^{12}\hat{s}^3 + 119M^{10}\hat{s}^4 - \right. \\ & \left. \left. 153M^8\hat{s}^5 - 17M^6\hat{s}^6 - 147M^4\hat{s}^7 - 8M^2\hat{s}^8 + 10\hat{s}^9 \right) \right). \end{aligned}$$

The gg production of $\chi_{c0,2}$ states, have collinear singularities. Performing regularization procedure (8), we obtain

$$\begin{aligned} \hat{\sigma}^{Reg}(gg \rightarrow \chi_{0g}) = & -\frac{2\pi\alpha^3 R_\chi'^2(0)}{3M^7\hat{s}^3 (M^2 - \hat{s})^4 (M^2 + \hat{s})^5} \left(99M^{24} + 132M^{22}\hat{s} - 7M^{20}\hat{s}^2 - \right. \\ & 80M^{18}\hat{s}^3 + 210M^{16}\hat{s}^4 - 560M^{14}\hat{s}^5 + 802M^{12}\hat{s}^6 + 696M^{10}\hat{s}^7 - \\ & 1721M^8\hat{s}^8 - 244M^6\hat{s}^9 + 789M^4\hat{s}^{10} + 56M^2\hat{s}^{11} + 12\hat{s}(-24M^{22} \\ & - 41M^{20}\hat{s} + 10M^{18}\hat{s}^2 + 7M^{16}\hat{s}^3 + 42M^{14}\hat{s}^4 - 176M^{12}\hat{s}^5 - 10M^{10}\hat{s}^6 + \\ & \left. 40M^8\hat{s}^7 + 14M^6\hat{s}^8 - 31M^4\hat{s}^9 + 9\hat{s}^{11}) \log \frac{M^2}{\hat{s}} - 172\hat{s}^{12} \right), \\ \hat{\sigma}^{Reg}(gg \rightarrow \chi_{2g}) = & -\frac{4\pi\alpha^3 R_\chi'^2(0)}{3M^7\hat{s}^3 (M^2 - \hat{s})^4 (M^2 + \hat{s})^5} \left(66M^{24} + 201M^{22}\hat{s} - \right. \\ & 31M^{20}\hat{s}^2 - 728M^{18}\hat{s}^3 + 360M^{16}\hat{s}^4 - 266M^{14}\hat{s}^5 + 256M^{12}\hat{s}^6 + 1032M^{10}\hat{s}^7 - \\ & 752M^8\hat{s}^8 - 271M^6\hat{s}^9 + 207M^4\hat{s}^{10} + 32M^2\hat{s}^{11} - 12\hat{s} \left(12M^{22} + 5M^{20}\hat{s} + 17M^{18}\hat{s}^2 + \right. \\ & 86M^{16}\hat{s}^3 - 204M^{14}\hat{s}^4 + 11M^{12}\hat{s}^5 + 31M^{10}\hat{s}^6 + 74M^8\hat{s}^7 - 8M^6\hat{s}^8 + 22M^4\hat{s}^9 - \\ & \left. \left. 6\hat{s}^{11} \right) \log \frac{M^2}{\hat{s}} - 106\hat{s}^{12} \right). \end{aligned}$$

3. $qg \rightarrow Qq$

At the qg channel the only χ_{cJ} mesons can be produced. The χ_1 meson cross section does not requires regularization and is equals to

$$\hat{\sigma}(qg \rightarrow \chi_1 q) = \frac{16\pi\alpha^3 R'_\chi{}^2(0)}{9M^7 \hat{s}^3} \left(4M^6 - 9M^2 \hat{s}^2 + 3M^4 \hat{s} \log \frac{\hat{s}}{M^2} + 5\hat{s}^3 \right). \quad (\text{A2})$$

Regularized cross sections for $\chi_{c0,2}$ are

$$\begin{aligned} \hat{\sigma}^{Reg}(qg \rightarrow \chi_0 q) &= -\frac{16\pi\alpha^3 R'_\chi{}^2(0)}{27M^7 \hat{s}^3} (4M^6 - 18M^4 \hat{s} + 57M^2 \hat{s}^2 + \\ &\quad 3\hat{s} (4M^4 - 9M^2 \hat{s} + 9\hat{s}^2) \log \frac{M^2}{\hat{s}} - 43\hat{s}^3), \\ \hat{\sigma}^{Reg}(qg \rightarrow \chi_2 q) &= -\frac{16\pi\alpha^3 R'_\chi{}^2(0)}{27M^7 \hat{s}^3} (20M^6 - 36M^4 \hat{s} + 69M^2 \hat{s}^2 + \\ &\quad 3\hat{s} (5M^4 - 12M^2 \hat{s} + 12\hat{s}^2) \log \frac{M^2}{\hat{s}} - 53\hat{s}^3). \end{aligned}$$

4. $q\bar{q} \rightarrow Qg$

At the $q\bar{q}$ channel, all cross sections are finite. This is explained by the fact, that their differential cross sections are cross-symmetric ($\hat{t} \leftrightarrow \hat{s}$) to the qg ones:

$$|\mathcal{M}(qg \rightarrow Qq)|^2 = |\mathcal{M}(q\bar{q} \rightarrow Qg)|^2 \Big|_{\hat{t} \leftrightarrow \hat{s}} \quad (\text{A3})$$

and the total cross sections are:

$$\hat{\sigma}(q\bar{q} \rightarrow \chi_0 g) = -\frac{128\pi\alpha^3 R'_\chi{}^2(0)}{81M^3 \hat{s}^3 (M^2 - \hat{s})} (\hat{s} - 3M^2)^2 \quad (\text{A4})$$

$$\hat{\sigma}(q\bar{q} \rightarrow \chi_2 g) = -\frac{256\pi\alpha^3 R'_\chi{}^2(0)}{81M^3 \hat{s}^3 (M^2 - \hat{s})} (6M^4 + 3M^2 \hat{s} + \hat{s}^2) \quad (\text{A5})$$

$$\hat{\sigma}(q\bar{q} \rightarrow \chi_1 g) = -\frac{256\pi\alpha^3 R'_\chi{}^2(0)}{27M^3 s^2 (M^2 - s)} (M^2 + s) \quad (\text{A6})$$

- [1] PANDA Collaboration (2007), hep-ex/0903.3905.
- [2] A. K. Likhoded, A. V. Luchinsky, Phys.Atom.Nucl. **71**, 294 (2008), hep-ph/0703091.
- [3] T. Alexopoulos et al. (E771), Phys. Rev. **D62**, 032006 (2000), hep-ex/9908010.
- [4] E. Braaten and J. Lee, Phys. Rev. **D67**, 054007 (2003), hep-ph/0211085.

- [5] V. G. Kartvelishvili, A. K. Likhoded, and S. R. Slabospitsky, Sov. J. Nucl. Phys. **28**, 678 (1978).
- [6] S. S. Gershtein, A. K. Likhoded, and S. R. Slabospitsky, Sov. J. Nucl. Phys. **34**, 128 (1981).
- [7] E. L. Berger and D. L. Jones, Phys. Rev. **D23**, 1521 (1981).
- [8] R. Baier and R. Ruckl, Phys. Lett. **B102**, 364 (1981).
- [9] R. Gastmans, W. Troost, and T. T. Wu, Nucl. Phys. **B291**, 731 (1987).
- [10] M. M. Meijer, J. Smith, and W. L. van Neerven, Phys.Rev. **D77**, 034014 (2007), hep-ph/0710.3090.
- [11] S. Alekhin, Phys. Rev. **D68**, 014002 (2003), hep-ph/0211096.
- [12] Stanley J. Brodsky , G. Peter Lepage, Paul B. Mackenzie, Phys. Rev. **D28**, 228 (1983).
- [13] O. Teryaev and A. Tkabladze, Phys. Rev. **D56**, 7331 (1997), hep-ph/9612301.
- [14] B. A. Kniehl, D. V. Vasin, and V. A. Saleev, Phys. Rev. **D73**, 074022 (2006), hep-ph/0602179.
- [15] S. P. Baranov, Phys. Rev. **D73**, 074021 (2006).
- [16] P. Hagler, R. Kirschner, A. Schafer, L. Szymanowski, and O. V. Teryaev, Phys. Rev. Lett. **86**, 1446 (2001), hep-ph/0004263.
- [17] A. K. Likhoded, V. A. Saleev, and D. V. Vasin, Phys. Atom. Nucl. **69**, 94 (2006).
- [18] L.-K. Ding and Q.-Q. Zhu, Phys. Lett. B **297**, 201 (1992).

